JOURNAL OF COMPUTATIONAL PHYSICS 107, 98–104 (1993)

# An Explicit Symplectic Integration Scheme for Plasma Simulations

J. R. CARY AND I. DOXAS

*Astrophysical Planetary and Atmospheric Sciences Department, University of Colorado, Boulder, Colorado 80309-0391*

Received May 20, 1992

An explicit symplectic integration scheme which describes the self-consistent wave particle interaction is developed. The integrator does not split the hamiltonian trivially into a kinetic and potential part. The integrator yields accurate growth rates for the gentle-bump instability even when the timestep is of the order of the inverse plasma frequency. This represents up to a tenfold reduction in computation compared to conventional schemes. The integrator is generalizable to arbitrary order without increase in storage requirements, but tests show that when the accuracy requirements are of the order of a few percent, the second-order method is the most efficient. 

## 1. INTRODUCTION

We have developed both second-order and fourth-order explicit symplectic integration schemes for the self-consistent interaction of charged particles with electrostatic waves. Symplectic integration schemes are those which preserve the Poincaré invariants and, as a result, are expected to have impoved stability. Previous work on hamiltonian formulations of particle simulations (e.g., Ref. [25]) effectively gave symplectic schemes for infinitesimal step size. Here we show how to advance symplectically particles and waves in a simulation with finite timestep.

We report accuracy studies for the analytically known problems of the cold beam [1] (one wave, cold beam) and the linear warm beam (one wave, warm beam). We find that for moderate accuracy ($\sim 5\%$) the method gives the correct mode growth rate and saturation frequency for timesteps of the order of the inverse plasma frequency, resulting in gains of up to an order of magnitude over the speed of fourth-order Runge–Kutta. For that level of accuracy, we find that the second-order method is the most efficient. We also observe that the total energy in the system is conserved very well (better than one part in $10^6$) for very long timesteps, although all other observables, including the growth rate, quickly diverge from their exact values for timesteps much greater than the inverse plasma frequency.

Symplectic integration has been known for some time [2], but recently there has been an explosion in the literature of symplectic integration methods [3–6]. Of particular interest are the new explicit integrators [7, 8, 26], which not only have all the good stability properties, but also require fewer force evaluations and less computer storage when the higher-order forms are used. These methods are rapidly being applied to many physical systems, including planetary evolution [9], the motion of charged particles in plasma confinement devices [10], and the study of plasma turbulence [11, 12].

The development of symplectic integration schemes is driven by the expectation that they will be more stable and that they will model more accurately the important features of hamiltonian systems when used with large timesteps. This expectation is raised by the KAM theorem, which states that symplectic approximations (for sufficiently small timestep) preserve most invariant sets and the nature of the motion on them. General symplectic integration methods are applicable whenever the dynamics is given by Hamilton's equations, as is the case for all fundamental interactions. *Explicit* symplectic integration methods can be used whenever the hamiltonian can be broken into several pieces, and Hamilton's equations for each of the pieces can be solved exactly. The leapfrog method, in which the hamiltonian is broken up into the kinetic and potential energy parts which are then advanced separately, is the simplest example.

In addition to their good stability properties, symplectic methods are also desirable because of the properties of their higher-order versions. Higher-order symplectic integration methods require no additional storage and fewer derivative evaluations than higher-order standard methods. Fourth-order Runga–Kutta, for example (e.g., Ref. [13]), requires the storage of two intermediate state vectors or state-vector differences, and four evaluations of the forces. By contrast, fourth-order symplectic schemes require no storage of intermediate values of the state vector, and only three evaluations of the forces. The first property allows one to consider higher-order methods in particle simulations for the first time.

In the following section we will describe briefly the physi-

0021-9991/93 $5.00

cal problem that motivated the work, and review previous analytical and numerical results for the restricted problem that we use to benchmark the code. In Section 3 we will describe the integration scheme and in Section 4 we will show our numerical results.

## 2. THE PHYSICAL PROBLEM

The integrator was developed to study the nonlinear stage of the self-consistent interaction of a weak warm beam with a cold background plasma [12]. In this section we describe the equivalent hamiltonian system used in our numerical experiments, and review previous analytical and numerical work done on the restricted problem of a cold beam.

A weak beam interacting with a background plasma will excite plasma waves in the part of the spectrum where $v(\partial f/\partial v) > 0$, where $f(x, v, t)$ is the distribution function. The part of the spectrum that will be subject to the instability, as well as the wave growth rate, are given by quasilinear theory [14, 15]. Although quasilinear theory has been accepted for so long that it is in the textbooks (e.g., Ref. [16]), recent theoretical work [17–19] indicates that it underestimates the wave growth rate by roughly a factor of two, even in the regime where its validity is generally accepted. As yet, no such discrepancy has been observed in experiments [20], but numerical work with both a test particle code [11] and the self-consistent code described here [12] indicates that there can indeed be an enhancement of the growth rate over quasilinear theory, although restricted to a smaller regime.

Traditionally, this and similar systems have been studied numerically using particle-in-cell techniques, but since the nonlinearity of the background plasma is unimportant, we follow Ref. [1] and study the equivalent system of charged particles interacting with electrostatic waves. The system can be described in hamiltonian form [21], and this is the formalism we use here. The hamiltonian formalism allows us to concentrate our computational resources on the evolution of the particles that form the tail of the distribution function, with no computational effort expended on the background plasma. It also allows us to compare our results with those of Ref. [1] for the cold beam case and even to study the linear warm beam–plasma instability, where a single wave interacts with a broad beam.

The hamiltonian describing the interaction of $N$ charged particles with $M$ electrostatic waves is given by [22]

$$H = \frac{1}{2}\sum_{i=1}^{N} p_i^2 + \frac{1}{2}\sum_{n=1}^{M} \omega_n (X_n^2 + Y_n^2) + \sqrt{\frac{2\eta}{N}} \sum_{i=1}^{N}\sum_{n=1}^{M} \frac{\beta_n}{k_n} \times [Y_n \sin(k_n x_i) - X_n \cos(k_n x_i)], \tag{1}$$

where $x_i$ and $p_i$ are the particle position and momentum, respectively, $\omega_n = \omega_p$ is the wave frequency (equal to the plasma frequency), $k_n$ is the wavenumber, $a_n = \frac{1}{2}\sqrt{X_n^2 + Y_n^2}$ is the wave amplitude, and $\phi_n = \arctan(Y_n/X_n)$ is its phase. The bulk of the plasma is a linear dielectric with dielectric constant $D(k, \omega)$ whose only function is to support the plasma waves, $\eta = n_b/n_p$ with $n_b$ and $n_p$ the beam and plasma number density, respectively, is the coupling constant, and $\beta_n$ is given by $\beta_n = [\partial D(k, \omega_n)/\partial \omega_n]^{-1/2}$, which in our case is $1/\sqrt{2}$ for all $n$ (we use a cold background plasma, so the plasma dielectric is given by $D(k, \omega) = 1 - \omega_p^2/\omega^2$).

The derivation of Eq. (1) relies on the amplitude variation being slow compared to the wave frequency. For collective oscillations this requires the frequency shift away from $\omega_p$ and the growth rate to be small compared to $\omega_p$. For random fluctuations, since the sum over $\sin(kx_i)$ goes as $N^{1/2}$, this gives the condition $\sqrt{2\eta}(\beta_n/k_n) \ll \omega_n a_n$, where $a_n = \frac{1}{2}\sqrt{X_n^2 + Y_n^2}$ is the wave amplitude.

The equations of motion for the above hamiltonian are

$$\begin{aligned}
\dot{x}_i &= \frac{\partial H}{\partial p_i} = p_i \\
\dot{p}_i &= -\frac{\partial H}{\partial x_i} = -\sqrt{\frac{2\eta}{N}} \sum_{n=1}^{M} [\beta_n Y_n \cos(k_n x_i) \\
&\quad + \beta_n X_n \sin(k_n x_i)] \qquad (2) \\
\dot{X}_n &= \frac{\partial H}{\partial Y_n} = \omega_n Y_n + \sqrt{\frac{2\eta}{N}} \sum_{i=1}^{N} \frac{\beta_n}{k_n} \sin(k_n x_i) \\
\dot{Y}_n &= -\frac{\partial H}{\partial X_n} = -\omega_n X_n + \sqrt{\frac{2\eta}{N}} \sum_{i=1}^{N} \frac{\beta_n}{k_n} \cos(k_n x_i).
\end{aligned}$$

The wave equations of motion are those for a harmonic oscilator with frequency $\omega_n$, whose amplitude is driven by particle currents at a rate controlled by the value of the coupling constant $\eta$.

In the following section we will outline the integration scheme. In Section 4 we will show that our integrator gives the correct linear growth rate for the cold beam model with timesteps of the order of the inverse plasma frequency (for a few percent accuracy). We will also show the evolution of a single wave interacting with a warm beam and show that the integrator gives the correct growth rate and resonance width for the wave with a timestep comparable to the inverse plasma frequency.

## 3. DESCRIPTION OF THE INTEGRATOR

The explicit symplectic integrator developed in Refs. [7, 8] for a hamiltonian $H(q, p) = H_1(q, p) + H_2(q, p)$

(see also [26] for a comprehensive description) is defined in terms of the transformations:

$$\begin{aligned} T_1(\tau) &= e^{-\tau L_1}, \qquad L_1 f = \{H_1, f\}, \\ T_2(\tau) &= e^{-\tau L_2}, \qquad L_2 f = \{H_2, f\}, \end{aligned} \tag{3}$$

where

$$L_j f = \{H_j, f\} = \frac{\partial H_j}{\partial q}\frac{\partial f}{\partial p} - \frac{\partial H_j}{\partial p}\frac{\partial f}{\partial q} \tag{4}$$

is the Poisson bracket of $H_j$ and $f$ with respect to $p$ and $q$. The method allows both $H_1$ and $H_2$ to depend on both $p$ and $q$, even though this may not be apparent in previous work. $T_1$ is the transformation that gives the exact evolution for $H_1$, while $T_2$ gives the exact evolution for $H_2$. If we denote by $T(\tau)$ the operator which advances the total hamiltonian $H$ exactly, then to second order in the timestep one has

$$T(\tau) = e^{-\tau L_H} = T_1(\tau/2)\, T_2(\tau)\, T_1(\tau/2) + O(\tau^3). \tag{5}$$

$T_1 T_2 T_1$ is symplectic since it is a product of symplectic operators. With $H_1 = H_1(p)$ and $H_2 = H_2(q)$, the above scheme is the leapfrog method. The generalization gives the new scheme the power needed to use longer timesteps, as we will see later.

To implement the integration scheme described above, we break the hamiltonian in Eq. (1) into two parts:

$$H_1 = \tfrac{1}{2}\sum_{i=1}^{N} p_i^2, \qquad H_2 = H - H_1. \tag{6}$$

Since $H_1$ depends only on the $p_i$, the transformation $T_1$ is trivial; the $X_n$, $Y_n$, and $p_i$ stay constant, and the $x_i$ are advanced with constant momenta,

$$T_1(\tau): x_i \to x_i + p_i \tau, \tag{7}$$

so the transformation $T_1$ advances the particle positions by free streaming.

The transformation $T_2$ is slightly more complicated. Since $H_2$ is independent of $p$, the $x_i$ are constant. We therefore have

$$\begin{aligned} \dot{X}_n &= \frac{\partial H}{\partial Y_n} = \omega_n Y_n + \sqrt{\frac{2\eta}{N}}\sum_{i=1}^{N}\frac{\beta_n}{k_n}\sin(k_n x_i) \\ &= \omega_n Y_n + S_n \\ \dot{Y}_n &= -\frac{\partial H}{\partial X_n} = -\omega_n X_n + \sqrt{\frac{2\eta}{N}}\sum_{i=1}^{N}\frac{\beta_n}{k_n}\cos(k_n x_i) \\ &= -\omega_n X_n + C_n, \end{aligned} \tag{8}$$

where the $S_n$ and $C_n$ are constants, since the $x_i$ are constant during $T_2$. If we now put $\bar{X}_n = C_n/\omega_n$ and $\bar{Y}_n = -S_n/\omega_n$, Eqs. (8) become

$$\begin{aligned} \frac{d}{dt}(X_n - \bar{X}_n) &= \omega_n (Y_n - \bar{Y}_n) \\ \frac{d}{dt}(Y_n - \bar{Y}_n) &= -\omega_n (X_n - \bar{X}_n); \end{aligned} \tag{9}$$

i.e., the waves are advanced as harmonic oscillators about a fixed centre $(\bar{X}_n, \bar{Y}_n)$. The solution of the above equations is then given by

$$\begin{aligned} X_n - \bar{X}_n &= (X_n^0 - \bar{X}_n)\cos\omega_n t + (Y_n^0 - \bar{Y}_n)\sin\omega_n t \\ Y_n - \bar{Y}_n &= (Y_n^0 - \bar{Y}_n)\cos\omega_n t - (X_n^0 - \bar{X}_n)\sin\omega_n t, \end{aligned} \tag{10}$$

where $X_n = X_n^0$ and $Y_n = Y_n^0$ at $t = 0$.

We can now advance the momenta. The equations of motion for the momenta

$$\begin{aligned} \dot{p}_i = -\frac{\partial H}{\partial x_i} &= -\sqrt{\frac{2\eta}{N}}\sum_{n=1}^{M} \\ &\times [\beta_n Y_n \cos(k_n x_i) + \beta_n X_n \sin(k_n x_i)] \end{aligned} \tag{11}$$

are easy to integrate using Eqs. (10) since the $x_i$ are constant. We find

$$\begin{aligned} \Delta p_i &= -\sqrt{\frac{2\eta}{N}}\sum_{n=1}^{M}\beta_n\left[\cos(k_n x_i)\int_0^\tau Y_n(t)\,dt \right. \\ &\quad \left. + \sin(k_n x_i)\int_0^\tau X_n(t)\,dt\right] \\ &= -\sqrt{\frac{2\eta}{N}}\sum_{n=1}^{M}\beta_n\left[\cos(k_n x_i)\left(\bar{Y}_n\tau + \frac{\Delta X_n}{\omega_n}\right)\right. \\ &\quad \left. + \sin(k_n x_i)\left(\bar{X}_n\tau - \frac{\Delta X_n}{\omega_n}\right)\right], \end{aligned} \tag{12}$$

where

$$\begin{aligned} \Delta X_n &= (X_n - \bar{X}_n)(\cos\omega_n\tau - 1) + (Y_n - \bar{Y}_n)\sin\omega_n\tau \\ \Delta Y_n &= (Y_n - \bar{Y}_n)(\cos\omega_n\tau - 1) - (X_n - \bar{X}_n)\sin\omega_n\tau \end{aligned} \tag{13}$$

so that the transformation $T_2$ is given by

$$\begin{aligned} X_n &\to X_n + \Delta X_n \\ Y_n &\to Y_n + \Delta Y_n \\ p_i &\to p_i - \sqrt{\frac{2\eta}{N}}\sum_{n=1}^{M}\beta_n[\cos(k_n x_i)(\bar{Y}_n\tau + \Delta X_n/\omega_n) \\ &\quad + \sin(k_n x_i)(\bar{X}_n\tau - \Delta Y_n/\omega_n)] \end{aligned}$$

$$\bar{X}_n = \frac{\sqrt{2\eta}\,\beta_n}{k_n\omega_n\sqrt{N}} \sum_{i=1}^{N} \cos(k_n x_i),$$
$$\bar{Y}_n = -\frac{\sqrt{2\eta}\,\beta_n}{k_n\omega_n\sqrt{N}} \sum_{i=1}^{N} \sin(k_n x_i). \tag{14}$$

The above scheme differs from the leapfrog method in that both wave coordinates are advanced together during $T_2$, the only approximation being that we consider the particle positions constant. The leapfrog method would advance the wave "positions" and their conjugate "momenta" ($X$ and $Y$, respectively) in alternate steps. Since the equations for the waves are coupled, there is really no leapfrog scheme for this problem (the hamiltonian cannot be separated into two parts of the form $H(p,q) = H_1(p) + H_2(q)$).

We have also developed a fourth-order integrator following Refs. [7, 8], which we will compare with the second-order one described above. The integrator is given by

$$T(\tau) = e^{-\tau L_H} \approx T_1(\alpha\tau)\, T_2(\beta\tau)\, T_1(\gamma\tau)\, T_2(\delta\tau) \times T_1(\gamma\tau)\, T_2(\beta\tau)\, T_1(\alpha\tau) + O(\tau^5), \tag{15}$$

where

$$\alpha = \frac{2 + 2^{1/3} + 2^{-1/3}}{6}$$
$$\beta = \frac{1}{2 - 2^{1/3}}$$
$$\gamma = \frac{1 - 2^{1/3} - 2^{-1/3}}{6} \tag{16}$$
$$\delta = \frac{1}{1 - 2^{2/3}}.$$

As can be seen from Eq. (15), the fourth-order method requires three evaluations of the forces per timestep, as opposed to only one for the second-order, and must therefore be able to use a timestep at least three times longer to break even in efficiency. As we will see in the next section, the fourth-order integrator can use a timestep twice as long as the second-order one for $\sim 5\%$ accuracy, so for that accuracy level the second-order method is most efficient.

## 4. NUMERICAL RESULTS

We have used the above scheme to study the analytically known problem of a cold beam [1] as well as the linear warm beam–plasma interaction (a warm beam interacting with only one wave) to demonstrate the accuracy of the new scheme. We find that we can obtain the wave growth rate, as well as the frequency of oscillation after saturation, to within $\sim 5\%$ using a timestep of the order of the inverse plasma frequency with the second-order method.

### 4.1. *The Cold-Beam Case*

The cold-beam model [1] applies when $\Delta v_b \ll \gamma_L/k$, where $\Delta v_b$ is the width of the beam. After a few exponentiations, an initially equally distributed spectrum of background noise will eventually be dominated by the fastest growing wave, whose phase velocity is calculated to be at

$$\delta v = \frac{1}{2}\left(\frac{\eta}{2}\right)^{1/3} v_b \tag{17}$$

away from the beam velocity $v_b$. This wave will grow exponentially with the linear growth rate until saturation, when it will trap the beam electrons and will begin to oscillate about a constant amplitude. The wave growth rate is calculated by linear theory to be

$$\gamma_L = \frac{\sqrt{3}}{2}\left(\frac{\eta}{2}\right)^{1/3} \omega_p, \tag{18}$$

where $\eta = n_b/n_p$ is the beam to plasma density ratio, and $\omega_p$ is the plasma frequency. The frequency of oscillation of the saturated wave is calculated numerically in Ref. [1] and is given by

$$\omega_b \approx \frac{4}{3}\left(\frac{\eta}{2}\right)^{1/3} \omega_p. \tag{19}$$

For the cold-beam case, we use 8000 particles interacting with a wave whose wavenumber is chosen to be unity, and we follow the wave amplitude in time. At $t = 0$ all particles have the same velocity $v_b = 1$. As a reference for our error estimates we use the results obtained with the fourth-order method and timestep $\omega_p \Delta t = 0.125$ ($\omega_p$ is the plasma frequency). We use that run as a reference because the results do not change if we reduce the timestep further and because the value of the growth rate and frequency of oscillation after saturation agree with Ref. [1]. The beam to plasma density ratio is chosen to be $\eta = 1.6 \times 10^{-8}$, so the theoretical growth time is $\tau_\gamma = 1/\gamma_L = 577$. With the reference run we find $\tau_\gamma = 578$ and $\omega_L = 2.62 \times 10^{-3}$, while the value for the frequency of oscillation after saturation found numerically in Ref. [1] is $\omega_b = 2.67 \times 10^{-3}$. The discrepancy in the value of the oscillation frequency is higher than that of the growth time because we had to read the value obtained in Ref. [1] off a small graph (they do not quote a numerical value).

Figure 1 shows the wave energy as a function of time for our reference run (fourth-order symplectic with $\omega_p \Delta t = 0.125$) drawn as a solid line, and the results of the second-order symplectic method for two different timesteps.

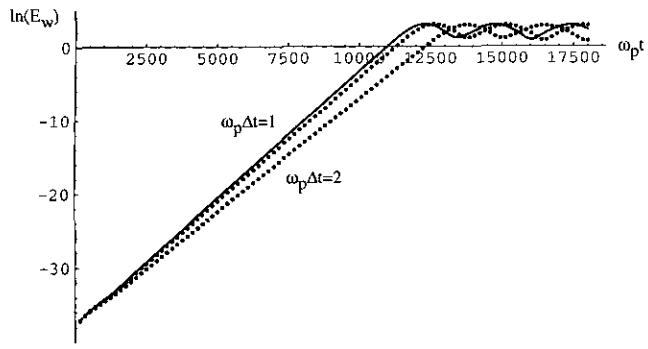


**FIG. 1.** The wave energy of the system described by Eq. (1) for the cold beam case, for two different values of the timestep (second-order method). The solid line is the result obtained with the fourth-order method and timestep $\omega_p \Delta t = 0.125$. The dotted curves are labeled with their respective timesteps.

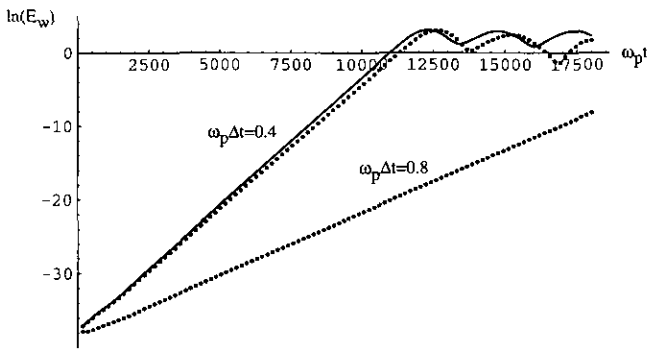


**FIG. 3.** The wave energy of the system described by Eq. (1) for the cold beam case. Two different values of the timestep using fourth-order Runge–Kutta. The solid line is the result obtained with the fourth-order symplectic method and timestep $\omega_p \Delta t = 0.125$ (same run as the solid line in Figs. 1 and 2). The dotted curves are labeled with their respective timesteps.

The second-order symplectic method is seen to give the growth rate and nonlinear frequency of amplitude oscillation to within 5% with a timestep of $\omega_p \Delta t = 1$. Increasing the timestep to $\omega_p \Delta t = 2$ does decrease the accuracy of the integration, but the simulation still gives qualitatively correct results. There is exponential growth followed by nearly dissipationless bounce oscillations.

The results of the fourth-order symplectic scheme are compared with the reference run in Fig. 2. The fourth-order scheme produces results accurate to 5% with a timestep of $\omega_p \Delta t = 2$. This timestep is longer than that for the second-order method, but not sufficiently to improve efficiency. As the fourth-order method requires three force evaluations per timestep rather than one, it actually requires 50% more computation at the 5% accuracy level. Since it is of higher order in $\Delta t$, it becomes inaccurate more quickly as the timestep is doubled to $\omega_p \Delta t = 4$, as is seen in Fig. 2.

Finally, we compare our results with fourth-order Runge–Kutta in Fig. 3. For a 5% error in the growth rate, Runge–Kutta requires a much smaller timestep, $\omega_p \Delta t = 0.4$. This means an increase in computation by a factor of 10, a factor of four because the Runge–Kutta method requires four force evaluations per timestep, and a factor of 2.5 from the decrease in the step size. Thus the symplectic integration scheme is an order of magnitude more efficient than this standard method. Figure 3 also shows that even at timestep $\omega_p \Delta t = 0.4$, the Runge–Kutta method obtains an amplitude value at the second minimum that is off by a factor of order unity. Finally, Fig. 3 shows that the fourth-order Runge–Kutta method goes rapidly bad with increased timestep, just like the fourth-order symplectic method.

Total energy conservation is often used to indicate when a simulation can be trusted. In Fig. 4 we plot the total energy versus time for the reference case, the second-order symplectic integrator with $\omega_p \Delta t = 10$, and the fourth-order Runge–Kutta with $\omega_p \Delta t = 0.4$. The second-order symplectic scheme is seen to conserve energy well long past the point (in $\Delta t$) where the calculated growth rates and frequencies become inaccurate (the symplectic integrator is not exactly energy conserving, because only the exact symplectic solu-

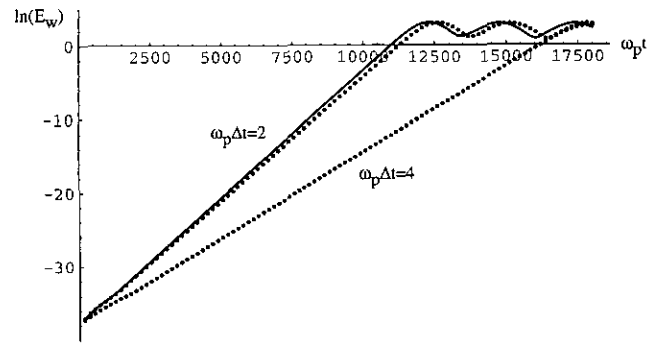


**FIG. 2.** The wave energy of the system described by Eq. (1) for the cold beam case. Fourth-order method, two different values of the timestep. The solid line is the result obtained with fourth-order and timestep $\omega_p \Delta t = 0.125$ (same run as the solid line in Fig. 1). The dotted curves are labeled with their respective timesteps.

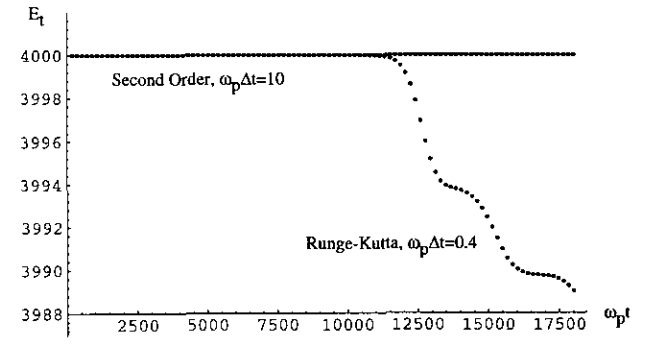


**FIG. 4.** The total energy of the system obtained with the symplectic method and with fourth-order Runge–Kutta. The solid line is the result obtained with the fourth-order symplectic method and timestep $\omega_p \Delta t = 0.125$ (same run as the solid line in Figs. 1–3). Dotted curves are labeled with their respective method and timestep.

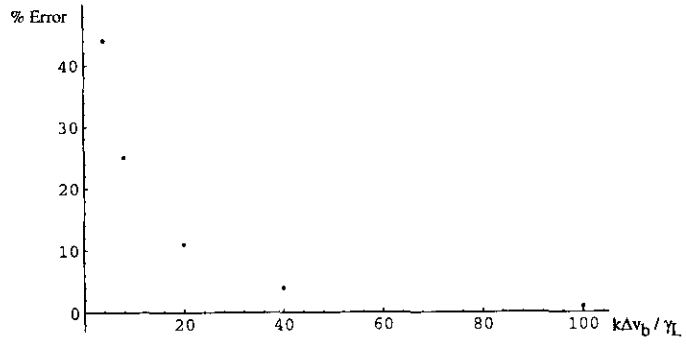


**FIG. 5.** The relative error in the value of the growth rate for the one wave warm beam case, as a function of the ratio $k\,\Delta v_b/\gamma_L$.

tion conserves energy [23]). Thus, energy conservation does not indicate accuracy of simulation. To some degree this can also be said of the Runge–Kutta integrator, which conserves total energy to approximately one part in 360 by the end of the simulation, yet gives a value for the wave amplitude at the second minimum that is off by a factor of order unity (cf. Fig. 3).

### 4.2. *The Warm-Beam Case*

For the case of a warm beam interacting with only one resonant wave, the growth rate is given by linear theory to be

$$\gamma_L = \frac{\pi}{2}\omega_p v^2 \frac{\partial f}{\partial v}, \tag{20}$$

where $f(x, v, t)$ is the particle distribution function and $\omega_p$ is the plasma frequency. The resonance half-width of the wave is given in terms of the parameters in the hamiltonian (1) by (see, e.g., Ref. [24])

$$\delta_r = 2\sqrt{\frac{a_n\beta_n}{k_n}}\left(\frac{2\eta}{N}\right)^{1/4}, \tag{21}$$

where $\eta = n_b/n_p$ is the beam to plasma density ratio, $a_n = \frac{1}{2}\sqrt{X_n^2 + Y_n^2}$ is the wave amplitude, and $\beta_n = 1/\sqrt{2}$ for a cold plasma. Equation (20) gives the wave growth rate, provided that

$$\frac{\gamma_L}{k} \ll \Delta v_b, \tag{22}$$

where $\Delta v_b$ is the width of the beam and $k$ is the wavenumber. The above condition means that the Fourier interaction width of the wave must be smaller than the width of the beam for the wave to be able to see the slope of the distribution function.

We find that condition (22) is actually quite restrictive. Figure 5 shows the percentage of error in the value of the growth rate as a function of the ratio $k\,\Delta v_b/\gamma_L$ ($k$ is equal to unity in this simulation). In order to obtain 1% accuracy, we need a ratio $k\,\Delta v_b/\gamma_L = 100$, which is the main reason we were forced to use so many more particles than in the cold-beam case.

In Fig. 6 we show our results for the linear warm-beam case (a warm beam interacting with a single wave). We use 512,000 particles with a distribution function given by

$$f(v) = C_1 + C_2\left(1 - \frac{v_1}{v}\right), \tag{23}$$

where $f(v) = 0$ outside the range $v_1 < v < v_2$. The coefficients $C_1$ and $C_2$ are obtained from normalization and from the linear growth rate $\gamma_L$ (cf. Eq. (20)), and are given by

$$C_2 = \frac{2\gamma_L}{\pi\omega_p\eta v_1^2}, \qquad C_1 = \frac{1 + C_2[v_1 \ln(v_2/v_1) - v_2 + v_1]}{(v_2 - v_1)}, \tag{24}$$

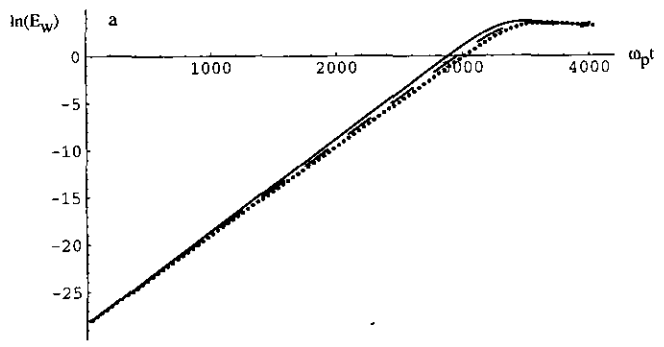


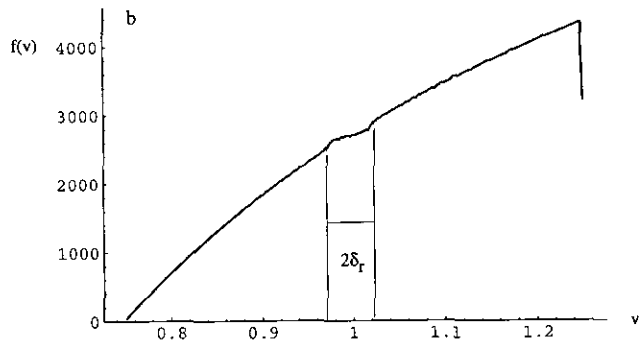


**FIG. 6.** The warm beam case with one wave: (a) shows the wave energy versus time. The solid line was obtained with the fourth-order method and $\omega_p\,\Delta t = 0.25$, the dotted line with the second-order method and $\omega_p\,\Delta t = 0.8$, and the dashed line with fourth-order Runge–Kutta and $\omega_p\,\Delta t = 0.45$; (b) the particle distribution function at $\omega_p t = 3250$ (obtained with the fourth-order symplectic method, $\omega_p\,\Delta t = 0.25$). The width of the region over which $f(v)$ is flatened, is approximately equal to the single mode resonance width at $\omega_p t = 3250$ (at which time $a_n = 6.33$).

where $\eta = n_b/n_p$ is the beam to plasma density ratio ($f(v)$ is normalized to $\eta$). For our run $k=1$, $\eta = 5.02\times 10^{-4}$, $v_1 = 0.75$, and $v_2 = 1.25$ with an initial linear growth time of $\tau_\gamma = 1/\gamma_L = 200$. The form of the distribution function was chosen so that the growth rate is constant over the entire velocity range.

Figure 6a shows the wave energy as a function of time for three different runs. The solid line is the reference run which uses the fourth-order method and timestep $\omega_p \Delta t = 0.25$. It gives $\tau_\gamma = 202$, within 1% of the theoretical value. The dotted curve was obtained with the second-order symplectic method and timestep $\omega_p \Delta t = 0.8$ and the dashed one with fourth-order Runge–Kutta and timestep $\omega_p \Delta t = 0.45$. The fourth-order symplectic method is found to give approximately 5% accuracy with $\omega_p \Delta t = 1.75$, and it is omitted from the graph for clarity. We see again that the symplectic methods can use timesteps of the order of the inverse plasma frequency for an accuracy level of approximately 5% and achieve computational savings of up to a factor of 7 over fourth-order Runge–Kutta.

The distribution function at $\omega_p t = 3250$ is shown in Fig. 6b. The width of the part of the distribution that is being flattened by the interaction with the wave is approximately $2\delta = 0.052$. This is within $\sim 7\%$ of the theoretical value $2\delta_r = 0.056$ of the wave resonance width at that time (cf. Eq. (21); at $\omega_p t = 3250$ the wave amplitude is $a_n = 6.33$).

## 5. CONCLUSIONS

We have developed and implemented second-order and fourth-order symplectic integration schemes for the self-consistent interaction of charged particles with electrostatic waves. For the 5% accuracy level typical of plasma simulations, we find that both schemes give good results with timestep of the order of the inverse plasma frequency, but that the second-order method is more efficient by a factor of $\sim 1.5$. Compared with conventional integration schemes (e.g., fourth-order Runge–Kutta) the new scheme is more efficient by up to an order of magnitude. We also find that total energy is well conserved even for timesteps of the order of $\omega_p \Delta t = 10$, when the integrator no longer foollows any observable accurately. Thus energy conservation is not an indicator of code accuracy.

## ACKNOWLEDGMENTS

This work was performed in part during our stay with the Equipe Turbulence Plasma. One of us (J.R.C.) was supported for five months by the Université de Provence, and the other (I.D.) for one year by the Commission of the European Communities. Computational resources were provided by the Conseil Scientifique du Centre de Calcul Vectoriel pour la Recherche and by the San Diego Supercomputer Center. Part of this work was supported by U.S. Department of Energy Grants DE-FG02-85 ER53207 and DE-FG02-86 ER40302. The authors wish to thank Dominique Escande for many fruitful discussions, and the Université de Provence for its hospitality during the course of this research.

## REFERENCES

1. T. M. O'Neil, J. H. Winfrey, and J. H. Malmberg, *Phys. Fluids* **14**, 1204 (1971).
2. R. DeVogelaere, Department of Mathematics, University of Notre Dame Report 4, 1956 (unpublished).
3. R. Ruth, *IEEE Trans. Nucl. Sci.* **30**, 2669 (1983).
4. F. Kang, *J. Comput. Math.* **4**, 279 (1986).
5. J. R. Cary, General symplectic integration algorithms through fourth order, *Bull. Am. Phys. Soc.* **34**, 1927 (1989).
6. P. J. Channel and C. Scovel, *Nonlinearity* **3**, 231 (1990).
7. E. Forest and R. D. Ruth, *Physica D* **43**, 105 (1990).
8. J. Candy and W. Rozmus, *J. Comput. Phys.* **92**, 230 (1991).
9. B. Gladman and M. Duncan, *Astron. J.* **100**, 1680 (1990).
10. J. R. Cary and J. A. Rome, "Symplectic Integration of Guiding-Center Orbits," Sherwood Theory Meeting, Gatlinburg, Tennesee, 1990.
11. J. R. Cary, D. F. Escande, and A. Verga, *Phys. Rev. Lett.* **65**, 3132 (1990).
12. J. R. Cary, I. Doxas, D. F. Escande, and A. D. Verga, *Phys. Fluids* **B4**, 2062 (1992).
13. W. H. Press, B. P. Flannery, S. A. Teukolsky, and W. T. Vetterling, *Numerical Recipes* (Cambridge Univ. Press, Cambridge, UK, 1986), p. 551.
14. A. A. Vedenov, E. P. Velikhov, and R. Z. Sagdeev, *Nucl. Fusion Suppl.* **2**, 465 (1962).
15. W. E. Drummond and D. Pines, *Ann. Phys. (N.Y.)* **28**, 478 (1964).
16. D. R. Nicholson, *Introduction to Plasma Theory* (Wiley, New York, 1983).
17. J. C. Adam, G. Laval, and D. Pesme, *Phys. Rev. Lett.* **43**, 1671 (1979).
18. G. Laval and D. Pesme, *Phys. Lett. A* **80**, 266 (1980); *Phys. Fluids* **26**, 52 (1983); *Phys. Rev. Lett.* **53**, 270 (1984).
19. K. Theilhaber, G. Laval, and D. Pesme, *Phys. Fluids* **30**, 3129 (1987).
20. S. I. Tsunoda, F. Doveil, and J. H. Malmberg, *Phys. Fluids B* **3**, 2747 (1991).
21. H. E. Mynick and A. N. Kaufman, *Phys. Fluids* **21**, 653 (1978).
22. D. F. Escande, in *Large-Scale Structures in Nonlinear Physics*, edited by J.-D. Fournier and P.-L. Sulem (Springer-Verlag, Berling, 1991), p. 73.
23. G. Zhong and J. E. Marsden, *Phys. Lett. A* **133**, 143 (1988).
24. B. V. Chirikov, *Phys. Rep.* **52**, 263 (1979).
25. H. R. Lewis, *Methods Comput. Phys.* **9**, 307 (1970).
26. H. Yoshida, *Phys. Lett. A* **150**, 162 (1990).